Microscopic and Anisotropic Dynamics of Spin Carriers with/without Charge

Kenji Mizoguchi

Dept. of Phys., Tokyo Metropolitan University, Hachi-oji, Tokyo 192-03, JAPAN

Abstract

Electron spin resonance (ESR) studies are reviewed, specifically focusing on an experimental parameter of frequency applied to organic conductive materials. By analyzing the ESR linewidth and/or the spin-lattice relaxation rate measured in a wide frequency range such as several MHz to 24 GHz, one can obtain a frequency spectrum of spin motion that gives characteristic parameters of such motion, anisotropic diffusion rates. The first example is a dynamics of so-called "neutral soliton" in trans-polyacetylene, which is a topological defect having spin half but no charge. In the case of polarons and/or conduction electrons in conducting materials, the dynamics of spin is equivalent to that of the charged carriers responsible for the electrical conduction. Polyaniline (PANI) and polythiophene (PT) are reviewed as examples of the conducting case with a quasi-one-dimensional electronic state. Recent development of this technique suggesting a new relaxation mechanism will be briefly mentioned.

1 Introduction

In most cases the electron spin resonance (ESR) has been studied as a function of temperature, while it has been rarely done over wide frequency range such as from 3 to 24,000 MHz [1]. Major reason to expand a frequency range of ESR has been to resolve origins of resonance shift, linewidth and relaxation and to investigate electronic states. So far, it is not adequately unveiled what kinds of information are embedded in the frequency axis, then it is interesting and important to survey a new world along the frequency axis. For example, in the case of pure Aluminum metal it was reported that the g-shift and the linewidth as functions of temperature and frequency exhibit anomalous behavior [2-4] and a new model for the g-shift and the linewidth in terms of the g-anisotropy in the k-space and the electron-electron correlation [3] was proposed to account for such anomalies. However, understanding remains still unclear [4] even in the pure Aluminum metal.

In this paper, ESR studies in the wide range of frequency will be reviewed especially to study the spin dynamics in conductive organic materials as successful examples [1]. Electron spins in these materials can move freely to convey charges. Such spins interact with other electron spins and nuclear spins through dipolar, exchange and hyperfine interactions. Spin motion modulates these interactions and produces a motion spectrum characteristic for the dimensionality of space where the spins are moving; frequency independent in the isotropic three dimension (3D), $\log\omega$ in the two dimension (2D) and $\omega^{-1/2}$ in the one dimension (1D). Then low dimensional systems, in other word, highly anisotropic electronic systems are interesting to apply the spin dynamics technique. Most cases frequently studied are the quasi-one dimensional systems (Q1D) where the characteristic motion spectrum $\phi(\omega)$ is expected to have an expression as follows [5, 6],

$$\phi(\omega)\approx\frac{1}{\sqrt{4D_{//}/\tau_{\perp}}}\sqrt{\frac{1+\sqrt{1+(\omega\tau_{\perp}/2)^2}}{1+(\omega\tau_{\perp}/2)^2}}, \qquad (1)$$

Springer Proceedings in Physics, Vol. 81
Materials and Measurements in Molecular Electronics
Editors: K. Kajimura · S. Kuroda

where $D_{//}$ is the diffusion rate along the one-dimensional axis, $\tau_{\perp}^{-1}$ the cutoff frequency that is, in some cases, equal to the diffusion rate perpendicular to the one-dimensional axis $D_{\perp}$, in unit of rad/sec for both diffusion rates, and ω the angular frequency. This spectrum can be measured by spin-lattice and spin-spin relaxation rates of ESR or NMR and yields above parameters for the anisotropic spin dynamics that can be reduced to the microscopic electrical conductivity even in polycrystalline materials. Here, only the case of ESR will be reviewed, then see recent reviews for other applications of the spin dynamics with both ESR and NMR [7, 8].

This review is organized as follows. Basic idea for background of the spin dynamics is mentioned in §2. In §3 experimental aspect is reviewed briefly. In §4, as a first example of the spin dynamics study, the neutral soliton dynamics in pristine *trans*-polyacetylene (*t*-PA) by the spin-lattice relaxation rate and the linewidth of ESR is demonstrated. The relaxation mechanism of ESR has been experimentally identified to eq. (1) in this system at first time. In §5, examples in conducting materials, polyaniline, polythiophene and polyheterocyclic polymers are demonstrated. In §6, recent findings that have a possibility to lead us to new information on the electronic states in conducting polymers and TTF-TCNQ will be described briefly and a conclusion in §7.

2 Background of spin dynamics

Idea to study the spin dynamics is based on detection of a motion spectrum that depends on the dimensionality of space where the spins are diffusing. Since the electron spins interact with the other electron spins and nuclear spins via dipolar and scalar couplings, the motion spectrum is generated as a local magnetic field randomly modulated by the spin motion. Such a motion spectrum can be measured by the spin-lattice or spin-spin relaxation rates that are proportional to the spectral density at the Larmor frequency ω_0. A functional form of the motion spectrum can be derived by a diffusion equation [5, 9] or a random walk formalism [6].

2.1 Autocorrelation function

The motion spectrum is described by a Fourier transform of an autocorrelation function $G(t)$ defined by [9]

$$G(t)=\iint p(\boldsymbol{r}_1)\Phi(\boldsymbol{r}_1,\boldsymbol{r}_2,t)F(\boldsymbol{r}_1)F^*(\boldsymbol{r}_2)d\boldsymbol{r}_1 d\boldsymbol{r}_2, \tag{2}$$

where $p(\boldsymbol{r}_1)$ is the probability density to find a spin at $\boldsymbol{r}_1$ and t=0, and $\Phi(\boldsymbol{r}_1, \boldsymbol{r}_2, t)$ the probability density to find such a spin at $\boldsymbol{r}_2$ after t. The $p(\boldsymbol{r}_1)$ is equal to the spin concentration c per unit molecule. $F(\boldsymbol{r})$ is the random function of the implicit parameter t, defined by the interaction Hamiltonian $\mathcal{H}_1=\Sigma_q F^{(q)}A^{(q)}$. In the case of dipolar interaction $F^{(q)}$ and $A^{(q)}$ are given by

$$F^{(0)}=\frac{1-3\cos^2\theta}{r^3}, \qquad A^{(0)}=-\frac{3}{2}\gamma_I\gamma_S\hbar\{-\frac{2}{3}I_zS_z+\frac{1}{6}(I_+S_-+I_-S_+)\}, \tag{3a}$$

$$F^{(\pm1)}=\frac{\sin\theta\cos\theta e^{\mp i\varphi}}{r^3}, \qquad A^{(\pm1)}=-\frac{3}{2}\gamma_I\gamma_S\hbar\{I_zS_\pm+I_\pm S_z\}, \tag{3b}$$

$$F^{(\pm2)}=\frac{\sin^2\theta e^{\mp 2i\varphi}}{r^3}, \qquad A^{(\pm2)}=-\frac{3}{4}\gamma_I\gamma_S\hbar I_\pm S_\pm, \tag{3c}$$

where r is the distance between two spins and θ the angle between the external magnetic field H_0 and the vector $\boldsymbol{r}$. The integration in eq. (2) means ensemble average taken over r in place of t.

2.2 Spectral density and dimensionality

Then the spectral density of the motion spectrum $J(\omega)$ is written by

$$J^{(j)}(\omega)=c\sum_{r_1,r_2}\phi(\boldsymbol{r}_1,\boldsymbol{r}_2,\omega)F^{(j)}(\boldsymbol{r}_1)F^{(j)*}(\boldsymbol{r}_2), \tag{4}$$

where $\phi(\boldsymbol{r}_1,\boldsymbol{r}_2,\omega)$ is a Fourier transform of $\Phi(\boldsymbol{r}_1, \boldsymbol{r}_2, t)$ and the sum is over r_1 and r_2 with all the possible sites. In the case of Q1D electronic systems providing that $\omega \ll D_{//}c_{//}^2/\Delta r_{\mathrm{eff}}^2$ where Δr_{eff} is the effective range of interaction [7], $\phi(\boldsymbol{r}_1,\boldsymbol{r}_2,\omega)$ is given by eq. (1) as a solution of the 1D diffusion equation $\partial\Phi/\partial t=\mathcal{D}_{//}\Delta\Phi$ modified by an escape probability from the chain, $\exp(-2t/\tau_\perp)$ [10]. Here, $\mathcal{D}_{//}$ (cm^2/s) is the diffusion coefficient, relating to the diffusion rate $D_{//}$ (rad/s) by $D_{//}=\mathcal{D}_{//}/c_{//}^2$, where $c_{//}$ is the intersite distance. Equivalently, anisotropic random walk formalism yielded the same result as the former approach [6]. In the two limits eq. (1) can be rewritten as

$$\phi(\omega)\approx\frac{1}{\sqrt{2D_{//}\omega}}, \qquad \text{for } 1/\tau_\perp \ll \omega \ll D_{//}, \tag{5a}$$

$$\phi(\omega)\approx\frac{1}{\sqrt{2D_{//}/\tau_\perp}}=\text{const.}, \qquad \text{for } \omega \ll 1/\tau_\perp. \tag{5b}$$

The former is of 1D regime and the latter is of 3D regime. The cutoff frequency $1/\tau_\perp$ is characterized as a crossover frequency between two regimes. $1/\tau_\perp$ is equal to the interchain diffusion rate $D_\perp$, providing that $D_\perp$ is the largest interaction between chains. In the case of chains with finite length, the cutoff frequency is shown to be dominated by the finite chain length effect instead of the interchain diffusion rate $D_\perp$ [7, 11].

2.3 Relaxation rates

The relaxation rates of ESR due to the Q1D spin motion are expressed by the spectral density of the motion spectrum $J^{(j)}(\omega)$ or that of the probability density $\phi(\omega)$ as

$$\begin{aligned}T_1^{-1}&=\frac{3}{2}\gamma_S^4\hbar^2S(S+1)[J^{(1)}(\omega_0)+J^{(2)}(2\omega_0)]\\&=\gamma_S^4\hbar^2S(S+1)c\Sigma_\ell[0.2\phi(\omega_0)+0.8\phi(2\omega_0)]\\&=3\gamma_S^2k_BT\chi\Sigma_\ell[0.2\phi(\omega_0)+0.8\phi(2\omega_0)],\end{aligned} \tag{6}$$

$$\begin{aligned}T_2^{-1}&=\frac{3}{8}\gamma_S^4\hbar^2S(S+1)[J^{(0)}(0)+10J^{(1)}(\omega_0)+J^{(2)}(2\omega_0)]\\&=\gamma_S^4\hbar^2S(S+1)c\Sigma_\ell[0.3\phi(0)+0.5\phi(\omega_0)+0.2\phi(2\omega_0)]\\&=3\gamma_S^2k_BT\chi\Sigma_\ell[0.3\phi(0)+0.5\phi(\omega_0)+0.2\phi(2\omega_0)]\end{aligned} \tag{7}$$

for the case of the electron-electron dipolar interaction [7, 9, 12], where γ_S is the gyromagnetic ratio of the electron spin and Σ_ℓ the lattice sum $\Sigma P_2(\cos\theta_{12})/(r_1^3r_2^3)$ [5]. The susceptibility χ is in units of emu/unit-molecule. In the second line of eqs. (6) and (7) the spectral density $J^{(j)}(\omega)$ is averaged out for the powder. Quantitative estimation of $D_{//}$ is not easy, since quantitative estimation of the lattice sum is required. On the other hand, quantitative estimation of the cutoff frequency is more accurate, since it depends only on the functional form of eq. (1). The spin-spin relaxation rate is directly related to the linewidth of ESR by a relation, $\Delta H_{\mathrm{pp}}=2T_2^{-1}/(\sqrt{3}\,\gamma_S)$ and composed of two parts; frequency-dependent $T_1'^{-1}\propto 0.5\phi(\omega_0)+0.2\phi(2\omega_0)$ (so-called life-time broadening because of the same origin as T_1^{-1}) and frequency-independent $T_2'^{-1}\propto 0.3\phi(0)$ (secular broadening). At the limit of 3D-regime, that is $\omega_0\approx 0$, eq. (6) becomes equal to eq. (7). Such equality was confirmed in pristine trans-polyacetylene [13]. Practically T_1^{-1} measurement is more difficult and tedious than T_2^{-1} and then the linewidth is usually used for the spin dynamics study.

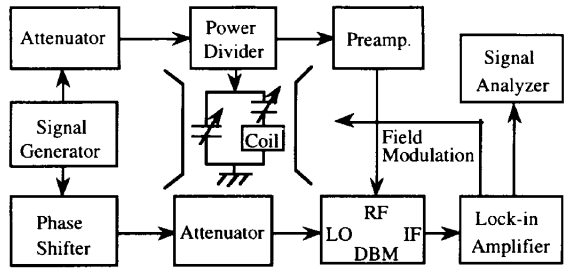

Fig. 1: A block diagram for ESR spectrometer.

3 Experimental

One of the key points of this experiment is to use one unique sample for all experiments over the studied frequency and temperature ranges, since ESR spectrum should be kept free from possible difference in a sample batch caused by any influence due to a presence of impurities such as oxygen and/or humidity, inhomogeneity of doping in different part of sample and etc. Generally samples are sealed into a quartz tube to avoid undesirable ESR signal from glass tube and any influence due to changes of circumstance. To gain sufficient sensitivity in the low frequency range down to several MHz, much more sample quantity than the case of a conventional ESR apparatus at X-band (~9 GHz) is required. We usually use a quartz tube with diameter of 5 mm that can be used up to 24 GHz. A block diagram of a homebuilt ESR spectrometer is shown in Fig. 1. Resonance circuit is composed of a coil and condensers in the lower frequency range than 1 GHz, a loop-gap resonator [14] in the higher frequency than 1 GHz and a cylindrical cavity at 24 GHz are used.

ESR spin-lattice relaxation rate T_1^{-1} is measured by a saturation method instead of a pulse method, since a dead time of signal receiving amplifier after high power *rf* pulses is more than 2 μs at 10 MHz and much longer than T_1 that is typically the order of less than 100 ns. An amplitude of *rf* magnetic field is calibrated by standard free-radical samples, (tri-p-nitrophenyl)methyl radical, $Q(TCNQ)_2$ or $Ad(TCNQ)_2$ where the spin-spin relaxation rate T_2^{-1} satisfies a relation $T_2^{-1}=T_1^{-1}$. When the temperature is changed, the amplitude of *rf*-magnetic field is monitored by a pick up coil located nearby the sample coil to keep accuracy of T_1^{-1} measurement.

ESR linewidth is defined as a peak-to-peak separation of absorption derivative. A least-square fitting with a Lorentzian lineshape is applied to deduce the linewidth from experimental data, which allows to determine the linewidth with resolution of the order of mG. In conductive materials the Lorentzian lineshape is commonly found because of rapid motion of charge carrier with spins which makes satisfy the condition for "the extreme narrowing limit" that assures the observation of the Lorentzian lineshape in ESR [8, 9].

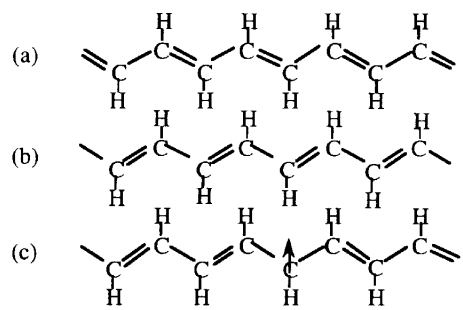

Fig. 2: The chemical structures for *trans*-polyacetylene, (a) phase A, (b) phase B and (c) neutral soliton as a zone boundary of phases A and B.

4 Pristine *trans*-polyacetylene -neutral soliton dynamics- [15-19]

As a good and successful example of the spin dynamics study, ESR investigation as a function of frequency in *trans*-polyacetylene is reviewed. Structure of *trans*-polyacetylene for different bond-alternation phases of A and B is shown in Fig. 2, together with the neutral soliton that is a zone boundary defect of the phases A and B, carrying spin 1/2 but no charge. In principle, the neutral soliton can move freely in the chain, since the ground state energy of the phase A is the same as that of B (degeneracy of ground states in bond alternation), so the energy of polymer chain is not influenced by a position of the neutral soliton. One of the evidences for such free motion of the neutral soliton is an observation of sharp ESR signal (less than 1 G) with Lorentzian lineshape, typical of motionally narrowed ESR spectrum [20]. The other evidence is an observation of the Overhauser effect [21-24], which is an enhancement of nuclear magnetization via saturation of ESR signal at the Larmor frequency of electron spin, $\omega=\omega_e$ [9, 25], providing that a correlation time of motion τ is enough shorter than $1/\omega_0 \approx 10^{-11}$ s. On the other hand, if the correlation time is longer than the inverse of hyperfine coupling frequency ($\approx 10^{-7}$ s), the solid state effect should be observed, which is also the enhancement of the nuclear magnetization, but the irradiation frequency of $\omega=\omega_e \pm \omega_n$ is required [7, 9]. The present study of the spin dynamics enables us to obtain quantitative information on the anisotropic motion of the neutral soliton as follows.

4.1 Frequency dependence of ESR T_1^{-1} and linewidth

Figure 3 shows the frequency dependence of the spin-lattice relaxation rate T_1^{-1} for *t*-$(CH)_x$ and *t*-$(CD)_x$. The concentration dependence of T_1^{-1} shown in Fig. 3 (b) provides important information to identify the relaxation mechanisms. The large intercept for *t*-$(CH)_x$ is reasonably ascribed to the hyperfine interaction with the proton, since the relaxation rate due to the hyperfine coupling with proton nuclei is larger than that with the deuteron by a factor of ≈ 16 in T_1^{-1} [12, 19]. The relaxation rate proportional to the spin concentration is consistent with the prediction of the electron-electron dipolar interaction described by eq. (6) (refer to the second line). The prediction of eq. (6) together with the hyperfine contribution reproduces the data well as shown by the solid curves in Fig. 3. According to eq. (7) it is also expected to find a similar frequency dependence for the ESR linewidth. Actually, the ESR linewidth shows a behavior predicted by eq. (7), as shown by the solid curves in Fig. 4. Characteristic features of this figure are

(.) that the slope of the solid curves gradually increases with decreasing temperature,

(2) that a constant contribution independent of frequency, corresponding to the intercept of the ordinate axis, rapidly increases with decreasing temperature, and

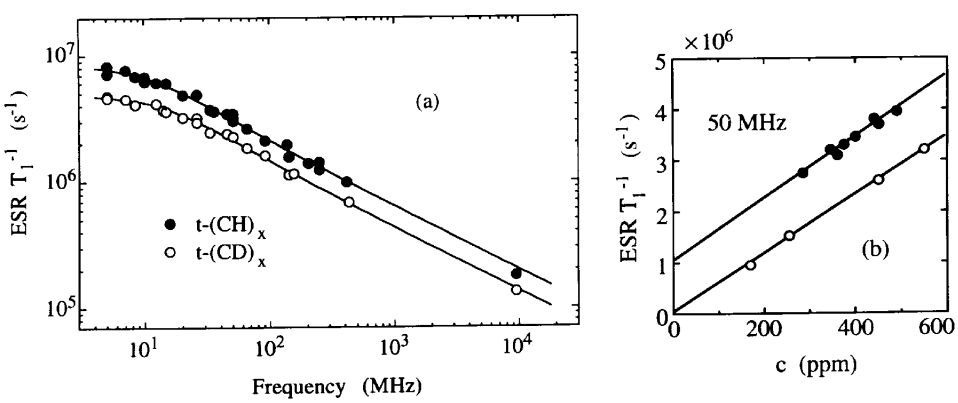

Fig. 3: (a) The frequency dependence of T_1^{-1} for *t*-$(CH)_x$ and *t*-$(CD)_x$. The solid curves indicate predicted behaviors of eq. (6). (b) The concentration dependence of T_1^{-1} for *t*-$(CH)_x$ and *t*-$(CD)_x$. (after K. Mizoguchi, K. Kume and H. Shirakawa, *Solid St. Commun.*, **50** (1984) 213-18)

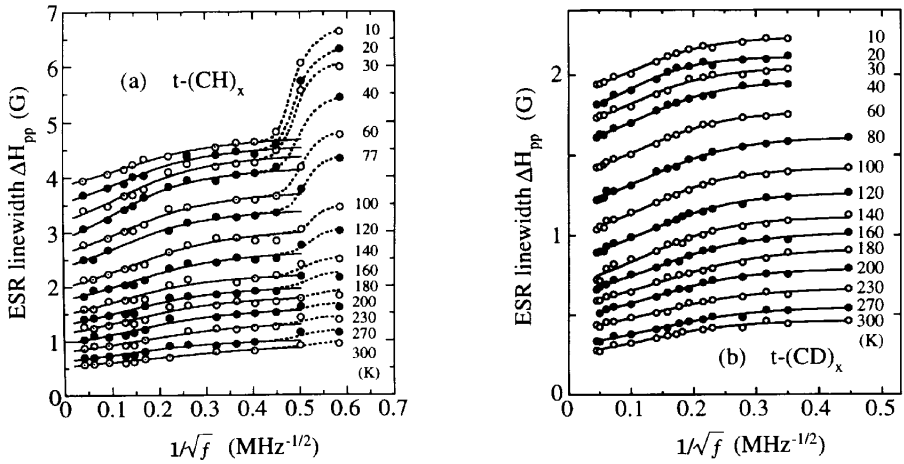

Fig. 4: ESR linewidth in (a) t-$(CH)_x$ and (b) t-$(CD)_x$ versus $1/\sqrt{f}$ with the implicit parameter of temperature. (after (a) K. Mizoguchi, S. Komukai, T. Tsukamoto, K. Kume, M. Suezaki, K. Akagi, and H. Shirakawa, *Synth. Met.*, **28**, 1989, D393-8 and (b) K. Mizoguchi, K. Kume, and H. Shirakawa, Synth. *Met.*, **17**, 1987, 439-45)

(3) that an anomalous steep broadening below 6 MHz (above $1/\sqrt{f}\approx 0.4$) is observed uniquely in t-$(CH)_x$ (refer to Fig. 6 for the lower frequency than $1/\sqrt{f}\approx 0.45$ in t-$(CD)_x$).

The first is interpreted by the Q1D motion of eq. (7), but the second requires to assume a diffuse/trap model for the neutral soliton dynamics proposed by Nechtschein et al. to account for the observed temperature dependence of ESR linewidth at X-band [23]. A schematic explanation for (1) and (2) in terms of the diffuse/trap model is shown in Fig. 5. When the neutral soliton is diffusing in normal sites, the linewidth broadens dynamically by the lifetime described by eq. (7). On the other hand, in a trapping site the linewidth broadens by spatial inhomogeneity of static local field, since the neutral soliton stays for longer duration than in the normal sites by several orders of magnitude. A criterion for the dynamic or static broadening is that the hopping rate of the spin is larger than the Larmor frequency or smaller than the hyperfine interaction frequency, respectively. Then, the diffuse/trap model requires that the linewidth is a sum of two contributions, dynamic and static broadenings, weighted by the ratio of duration being diffusing and trapped as shown in Fig. 5. As the origins of the trapping several possibilities have been proposed [7, 26].

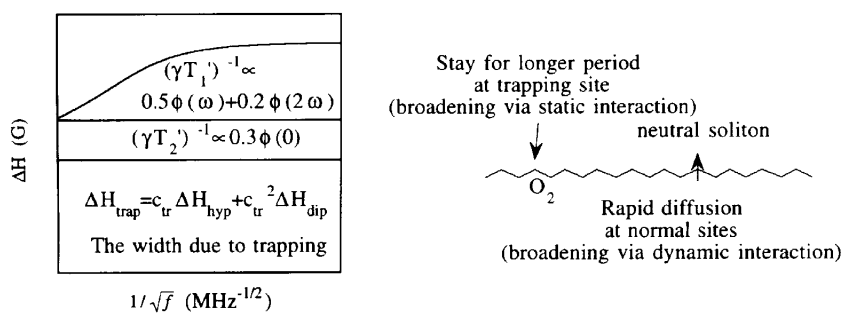

Fig. 5: A schematic figure for the origin of ESR linewidth in terms of the diffuse/trap model. ΔH_{hyp} and ΔH_{dip} are the static broadening due to hyperfine and electron-electron dipolar interactions, respectively. c_{tr} is the ratio of duration stay at the trapping site, $t_{tr}/(t_{tr}+t_{diff})$.

4.2 Anomalous broadening below 6 MHz in *t*-$(CH)_x$

The above understanding helps us to interpret the anomalous broadening below 6 MHz found uniquely in *t*-$(CH)_x$. The nature of this anomaly appears in the characteristic pattern of the linewidth against the angle of the external magnetic field to the chain axis in stretch-oriented films of both *t*-$(CH)_x$ and *t*-$(CD)_x$ as shown in Fig. 6. Some characteristic indications are found

(1) in the reversed phase of anisotropy in the protonated and deuterated polyacetylenes, and

(2) in the strong enhancement of the anisotropy in the protonated polyacetylene.

The reversed phase is well evidenced that the phase of *t*-$(CD)_x$ comes from the dynamic origin shown by eq. (7) and that the other phase of *t*-$(CH)_x$ does from the static one produced during the trapping [16, 27, 28] because of the larger hyperfine width than *t*-$(CD)_x$. Then, the anomaly in the linewidth is ascribed to the enhancement of the width due to trapping. The reason why such an enhancement appears below 6 MHz solely in *t*-$(CH)_x$ is due to a crossover from "unlike" spins to "like" spins in the electron and nuclear coupled spin system. Usually the static coupling is caused by $aS_z \cdot I_z$ term that conserves total energy of the spin system even for the "unlike" spins, but not by $bS_{\pm} \cdot I_{\mp}$ term due to decoupling by the large Zeeman energy splitting under strong external field. However, under the special condition of Larmor frequency f less than 6 MHz, the spin system becomes "like" spins because of mixing due to the larger hyperfine coupling frequency A ($\mathcal{H}=2\pi\hbar AS \cdot I$) than the Larmor frequency. Therefore, $bS_{\pm} \cdot I_{\mp}$ term becomes effective to broaden the ESR linewidth below 6 MHz [19]. Using this crossover frequency the maximum spin density ρ of the neutral soliton can be deduced. The effective hyperfine coupling constant $A_{eff}=A \cdot \rho/2=6$ MHz with $A=-70$ MHz/spin yields ρ to be 0.17 spins/carbon at the center of the neutral soliton extension spread over 18 CH units [29, 30], in good agreement with the ENDOR result in *cis*-polyacetylene [29, 30]. Finally in the case of the deuterated polyacetylene because of the smaller nuclear moment than that of proton, a similar enhancement of the linewidth could be expected if the Larmor frequency were reduced to the comparable magnitude to that of the electron-deuteron coupling.

4.3 Temperature dependence of diffusion rates

With the least square fitting as demonstrated by the solid curves in Figs. 3 and 4, the temperature dependence of the diffusion rate along the chain $D_{//}$ and the cutoff frequency (the diffusion rate across the chains) were derived as shown in Fig. 7, where the correction arising from the trapping was made [19, 23]. The thick solid curve shows $D_{//}$ without correction of the trapping, which indicates importance of the correction below 100 K. Such a correction for the proton NMR entirely

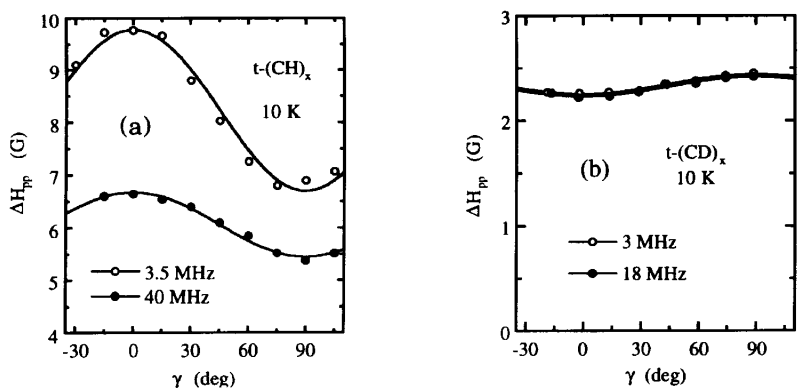

Fig. 6: Angular dependence of the ESR linewidth (a) at 3.5 and 40 MHz for *t*-$(CH)_x$ and (b) at 3 and 18 MHz for *t*-$(CD)_x$, at 10 K. Note the reversed phase of anisotropy pattern each other. (after K. Mizoguchi, S. Komukai, T. Tsukamoto, K. Kume, M. Suezaki, K. Akagi, and H. Shirakawa, *Synth. Met.*, **28**, 1989, D393-8)

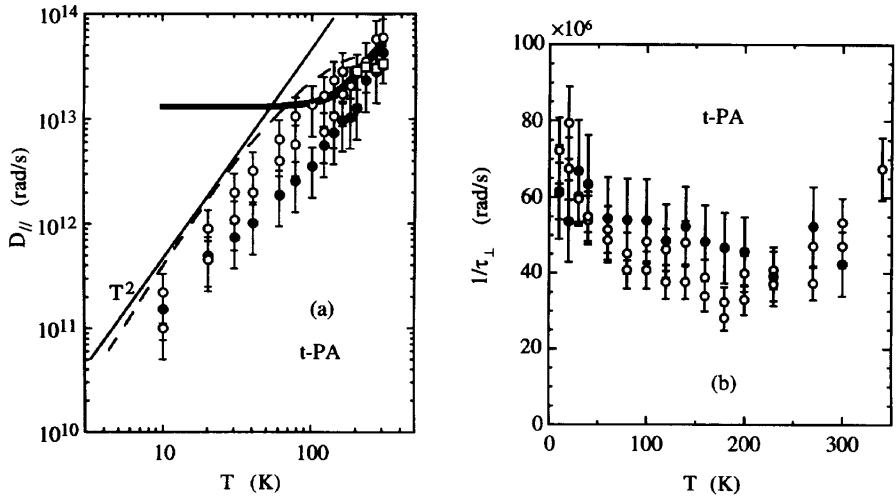

Fig. 7: The temperature dependence of the diffusion rate (a) along the chain and (b) across the chains. ○ *t*-$(CD)_x$, ● *t*-$(CH)_x$ (ESR linewidth), ❑ *t*-$(CD)_x$, (ESR T_1^{-1}) and --- *t*-$(CH)_x$ (NMR T_1^{-1}) [23]. (after K. Mizoguchi, S. Masubuchi, K. Kume, K. Akagi, and H. Shirakawa, *Phys. Rev.*, **B51**, 1995, 8864-73)

changes the original behavior to give the corrected result shown in Fig. 7 (a) [23]. The obtained temperature dependence of $D_{//}$ with both ESR and NMR shows good agreement with each other, suggesting rationality of the present experiment and analysis with the diffuse/trap model. Such a temperature variation of $D_{//}$ implies that at absolute zero the neutral soliton is fixed even at the normal sites and that the scattering with phonons activate its diffusion below 300 K. These behaviors can be compared with the theoretical considerations [31-37]. On the cutoff frequency there are several possibilities, hopping of the spins between chains, exchange coupling and spin-spin relaxation itself [38]. The cutoff frequency shows weak variation against the temperature as shown in Fig. 7 (b). The decrease with increasing temperature up to 100 K can be ascribed to motion induced invalidation of exchange coupling among the nearby neutral solitons fixed around the trapping center at absolute zero. Above 200 K it is probable that the hopping of the neutral soliton between the chains could be activated thermally, for example via charged solitons created by unexpected doping as predicted by Kivelson [39], although a serious question of validity of this mechanism has been raised [40]. Here, note that the anisotropy of the neutral soliton dynamics is as large as 10^6, consistent with the topological nature of the neutral soliton.

5 Conducting state of polymers

5.1 Polyaniline (PANI) [41-44]

Polyaniline is a stable conducting polymer in air with chemical structure shown in Fig. 8 and shows the electrical conductivity up to several hundredth S/cm at 300 K by protonating with HCl and camphorsulfonic acid (CSA) [45-47]. It is known that crystalline structure of PANI is not only depends on species of counter ions, but also on sample morphology, powder or film [48-50]. PANI powder protonated with HCl by dipping in aqueous solution of HCl, has ES-I structure, but a four-fold stretch-oriented PANI film cast from N-methylpyrrolidinone (NMP) solution shows ES-II structure [48] with the higher electrical conductivity than in ES-I. In this section the spin dynamics study to clarify microscopic and anisotropic charge conduction in the ES-I powder is reviewed [41-44].

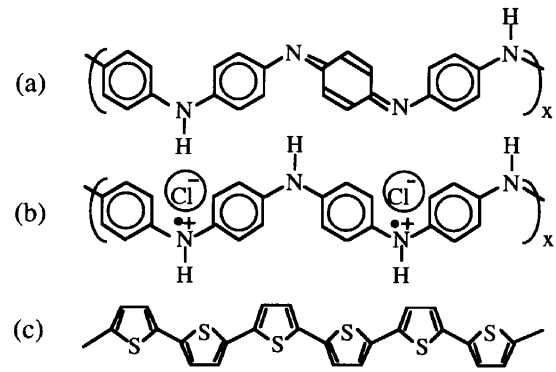

Fig. 8: Chemical structures of (a) neutral (Emeraldine base form, EB) and (b) oxidized (Emeraldine salt form, ES) polyanilines. ES is protonated with HCl. (c) polythiophene. Protons bonded to carbon atoms are abbreviated.

5.1.1 Protonation dependence

Figure 9 (a) shows the ESR linewidth as a function of $1/\sqrt{f}$ [1]. Note that the cutoff frequency $1/\tau_\perp$, crossover frequency from 1D to 3D regime, remarkably increases from $1/\sqrt{f}\approx 0.15$ ($\approx$50 MHz) to 0.01 ($\approx$10 GHz) at y$\approx$02~0.3. On the other hand, $D_{//}$ is almost independent of y as found in Fig. 9 (b). These findings can be understood as a percolative transition due to segregative protonation, in agreement with the conclusion drawn from the Pauli-like susceptibility increasing proportionally with y [52]. ESR observes the spin carriers on the particular chains fully protonated segregatively and other unprotonated chains have no spin carriers, resulting in a single value for $D_{//}$ independent of y. In the same time, the percolative connection of chains strongly enhances the interchain diffu-

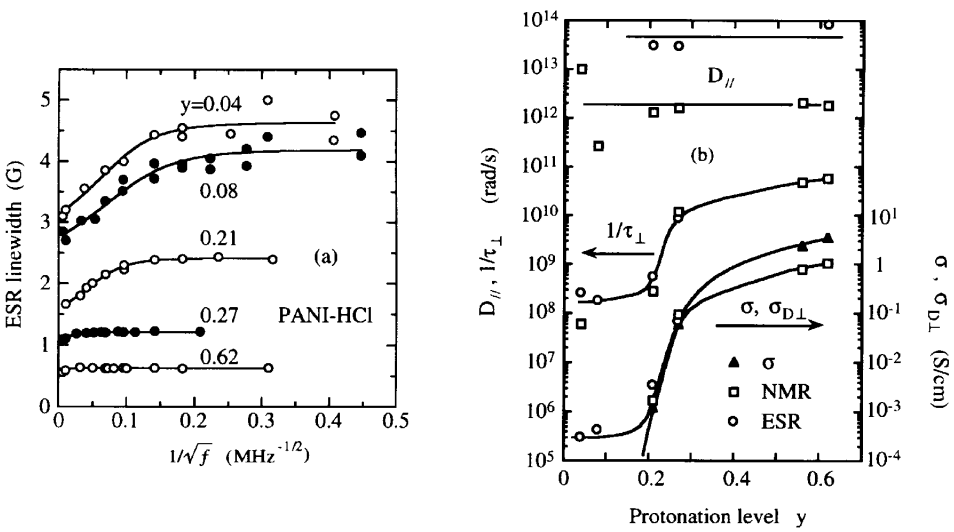

Fig. 9: (a) The frequency dependence of the ESR linewidth with an implicit parameter of protonation level y. (b) The diffusion rate $D_{//}$ and the cutoff frequency $1/\tau_\perp=D_\perp$ with the dc conductivity and the microscopic conductivity deduced from $D_\perp$ against y. Origin of a quantitative difference of $D_{//}$ for ESR from for NMR is probably that each of ESR and NMR requires estimation of similar but different quantities from each other to calculate $D_{//}$. A leveling off of $1/\tau_\perp$ below y$\approx$0.2 is ascribed to the other mechanism than the interchain hopping rate $D_\perp$ for the cutoff frequency $1/\tau_\perp$ [51]. (after K. Mizoguchi, *Jpn. J. Appl. Phys.*, **34**, 1995, 1-19)

sion rate $D_\perp$ ($=1/\tau_\perp$) at y≈0.2~0.3 that corresponds to the percolation threshold p_c≈0.4~0.6. Such a value of p_c is reasonable because the effective dimensionality for the percolation of the interchain hopping is two dimensional triangular lattice that has p_c=0.5 because polyacetylene chain has six neighboring chains at nearly equidistance. The other important feature of Fig. 9 (b) is the protonation dependence of microscopic conductivity $\sigma_{D_\perp}$ derived from $D_\perp$ for the charge carriers with spin, using Einstein relation $\sigma_{D_\perp}=e^2N(E_F)D_\perp c_\perp^2$ for systems with Pauli susceptibility. Here, $N(E_F)$ is the density of states at the Fermi energy and $c_\perp$ the interchain distance. $\sigma_{D_\perp}$ behaves very correspondingly to the dc conductivity measured in the same sample as demonstrated in Fig. 9 (b), which claims that the dc conductivity of PANI-HCl powder is limited by the interchain hopping rate $D_\perp$. Such a correspondence is found also in the temperature dependence of the conductivity [43, 44].

5.1.2 Temperature dependence [44, 53]

The temperature dependence of the ESR linewidth with an implicit parameter of frequency is plotted in Fig. 10 (a) for PANI-HCl with y=0.62. One feature is that the lower the frequency, the larger the temperature dependence, particularly below 100 K. In other words, the lower the temperature, the larger the frequency dependence of the linewidth. This frequency dependence can be ascribed to the quasi-one dimensional motion of the spins [44, 53]. Such an analysis of the frequency dependence yields the residual linewidth corresponding to "the observed linewidth-eq. (7)", which is plotted by the open diamonds in Fig. 10 (a). Origin of the residual linewidth is not clear, but recently new model on the collision with oxygen were proposed [8, 54]. According to this, the line broadening δ_{ox} is proportional to $pC_BD_{//}$, where C_B is the concentration of oxygen and p the efficiency of collision. In the case of "strong collision" via exchange interaction, which forces to lose phase memory of the spin carrier, $\delta_{ox}\propto C_BD_{//}$ since p is constant. On the contrary, if the scattering center works for "weak collision", $\delta_{ox}\propto C_B/D_{//}$ since $p=1/D_{//}^2$. Then, actual line broadening depends on the nature of interactions, "strong" or "weak". Realistically, distance between the charge carrier and the oxygen would distribute over the size of microscopic crystal; the shorter the distance, the stronger the collision, but the longer the distance, the weaker the collision. Therefore, the expected dependence on the diffusion rate $D_{//}$ for the line broadening is dominated by the average "collision strength" and the shape of its distribution. Following such a consideration, we examined the temperature dependence of the residual linewidth to fit with the diffusion rate $D_{//}$ (as indicated by the

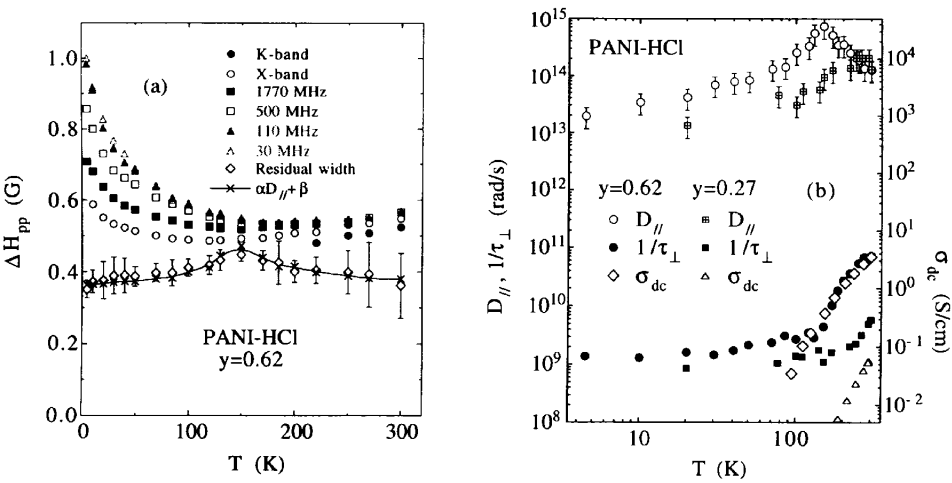

Fig. 10: (a) The temperature dependence of the ESR linewidth with an implicit parameter of frequency. (b) The temperature dependence of the diffusion rate $D_{//}$ and $1/\tau_\perp$. Reason why $1/\tau_\perp$ levels off around 10^9 is the same as the case in Fig. 9(b). (for (b), after K. Mizoguchi and K. Kume, *Synth. Met.*, **69**, 1995, 241-2)

open circles in Fig. 10 (b)) deduced by the Q1D fitting applied to the frequency dependence shown in Fig. 10 (a). The solid curve in Fig. 10 (a) shows a formula $\alpha D_{//} + \beta$ (G) which well reproduces the residual linewidth with $\alpha = 1.5 \times 10^{-16}$ (G•s) and $\beta = 0.36$ (G). This result enables us to conclude that the "strong collision" dominates the residual linewidth, together with the temperature independent width, in other words, the width independent of $D_{//}$. It is possible that the broadening becomes independent of the diffusion rate $D_{//}$ because an average of p becomes proportional to time interacting with oxygen, that is $p = 1/D_{//}$ and then δ_{ox}=const., if one takes into account a distribution of the coupling strength, as in the case of the transition probability in magnetic resonance [9].

Fig. 10 (b) shows some characteristic features that PANI-HCl with y=0.62 shows semiconducting-to-metallic transition around 150 K, but the sample with y=0.27 shows semiconducting behavior up to 200 K. The transition temperature seems to move to higher temperature with decreasing y. Such a microscopic conductivity shows a completely different behavior from the dc conductivity that is governed by the interchain hopping rate $D_{\perp}$, as clearly demonstrated in Fig. 10 (b) for both y=0.62 and 0.27. Here, note a difference of the scales; the left scale for $1/\tau_{\perp}$ and the right for σ_{dc} in Fig. 10 (b). Another point is a large anisotropy ratio of $D_{//}/D_{\perp}$, more than 10^3 for y=0.62 and 10^4 for y=0.27 at 300 K and reaches more than 10^4 at 150 K. Such a large anisotropy yields an estimation of chain length to be $l_{min} = \sqrt{D_{//}/D_{\perp}}\, c_{//} \approx (3 \times 10^4)^{1/2} c_{//} = 180 c_{//}$ resulting from a finite chain length effect [1]. This value is consistent with the average molecular weight of 50,000 for PANI [55]. Similar consideration for *trans*-polyacetylene yields $l_{min} \approx 10^3 c_{//}$.

5.2 Polythiophene (PT) [56, 57]

Another example of polythiophene (see, Fig. 8 (c) for chemical structure) applied the spin dynamics study is reviewed [56-58]. PT-ClO_4^- is prepared by electrochemical oxidation in inert atmosphere [58] so that the broadening due to oxygen can not be expected as in the case of PANI-HCl. The frequency dependence of the ESR linewidth is shown in Fig. 11 (a). In this polymer there are three different origin of the linewidth, Q1D (eq. (7)), Elliott mechanism and anisotropic g-shift.

The Elliott mechanism [59] induces a spin-flip scattering via a spin-orbit interaction, which is proportional to the momentum relaxation rate $1/\tau_r$ due to phonon scattering. Since such a relaxation rate $1/\tau_r$ dominates the electrical resistivity ρ, the Elliott broadening ΔH_{Ell} is expected to correspond to the resistivity ρ. Figure 11 (b) demonstrates a good correspondence between the linewidth and the voltage-shorted-compaction (VSC) resistance [60], which suggests the electronic state of this system is metallic consistent with an observation of the Pauli-like susceptibility [56, 57, 61, 62] and

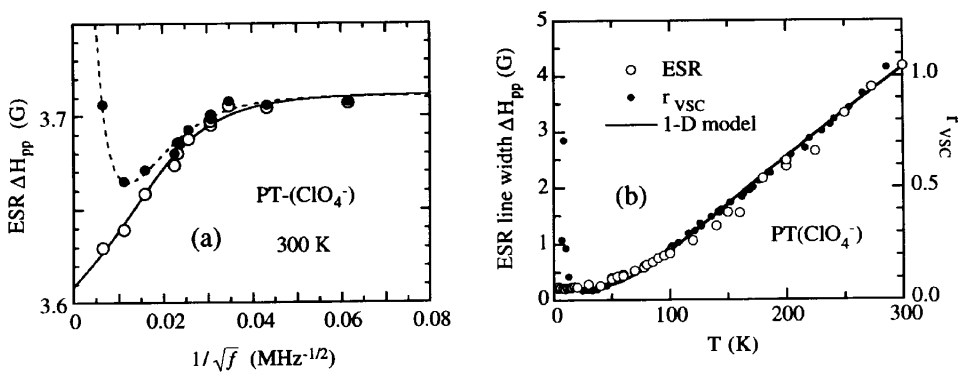

Fig. 11: (a) The frequency dependence of the ESR linewidth and (b) the temperature dependence of the ESR linewidth for Polythiophene doped by ClO_4^-, together with the VSC resistance ratio [60]. (after (a) K. Mizoguchi, M. Honda, S. Masubuchi, S. Kazama, and K. Kume, *Jpn. J. Appl. Phys.*, **33**, 1994, 971-5 and (b) K. Mizoguchi, M. Honda, N. Kachi, F. Shimizu, H. Sakamoto, K. Kume, S. Masubuchi, and S. Kazama, *Solid St. Commun.*, **96**, 1995, 333-7)

Table I. The parameters for polythiophene obtained at 300K from the analysis of ESR broadening due to the diffusive motion and the Elliott mechanism. D is the diffusion rate, τ_r the relaxation time for scattering, V_F the Fermi velocity, ℓ^* the mean free path and σ the electrical conductivity. (after K. Mizoguchi, M. Honda, S. Masubuchi, S. Kazama, and K. Kume, *Jpn. J. Appl. Phys.*, **33**, 1994, 971-5)

	D (rad/s)	τ_r (s)	V_F (cm/s)	ℓ^* ($c_{//}$ or $c_\perp$)	σ (S/cm)
//	1.9×10^{15}	5×10^{-16}	8.0×10^{7}	≈1	1.2×10^{3}
$\perp$	5.5×10^{9}				0.037

linear thermoelectric power [58, 60, 63]. Both the linewidth and the VSC resistance behave as T^2 at lower temperature than 100 K and approach a linear dependence at higher temperatures, which can be understood by a simple 1D metal model [64-66]. Further evidence of the Elliott broadening is found that the linewidth at 300 K shows an expected behavior of the Elliott mechanism, that is, clear proportionality to λ^2, where λ is the spin-orbit coupling constant for the heaviest atoms in not dopant but the polymer backbone of various heterocyclic polymers with five members, such as polythiophene, poly(3-methylthiophene) and polypyrrole doped by a series of dopants [7, 56]. Similar dependence on λ of the alkali metal dopants was reported for other conducting systems, such as polyacetylene [67-69], poly-p-phenylene [70], graphite intercalated compounds (GIC) [71] and fullerides [72]. To validate the Elliott mechanism it requires some deviation from the pure-one-dimensional symmetry in the electronic state; heterocyclic polymers have molecules with asymmetric structure and other alkali-doped systems have sizable contribution of alkali ions.

The broadening due to the g-shift anisotropy is inhomogeneous broadening proportional to the Larmor frequency and arises only in polycrystalline samples, since ESR signal from each crystal with different direction of the crystal axis appears at different magnetic field strength. The most prominent contribution to the ESR linewidth is the Elliott broadening which gives information on the scattering rate $1/\tau_r$ with phonons. The diffusion rates $D_{//}$ and $D_\perp$ deduced from the solid curve in Fig. 11 (a), can be combined with the scattering rate $1/\tau_r$ to give several parameters on the electronic state in PT-ClO_4^- [1, 57], as listed in Table I.

6 Recent findings

As another application of the frequency dependence of ESR, an organic charge transfer salt TTF-TCNQ was investigated, in relation to the NMR result studied as a function of frequency [10]. Although the reported NMR data claimed that the relaxation rate is dominated by Q1D mechanism, the ESR linewidth showed no such a dependence proportional to $1/\sqrt{f}$, instead the linewidth was rather proportional to $f\sim f^2$ and leveled off around 50 MHz, keeping constant up to 2,000 MHz as shown in Fig. 12 (a). A similar behavior, but smaller amplitude, has also been found in PANI-HCl film cast from NMP solution (Fig. 12 (b)) and PANI-CSA (camphorsulfonic acid) cast from *m*-cresol solution. In general, the spectral density of the local field approaches zero with the frequency goes to infinite. However, it can occur when the local field strength is proportional to the frequency. One example is the hopping of the spins between TTF and TCNQ stacks with the different g-values, but it is easily shown to be too small in magnitude. Similar mechanism was proposed to explain the anomalous frequency dependence of g-shift in pure aluminum that the g-anisotropy on the Fermi surface combined with the electron-electron correlation could yield the expected frequency dependence [3, 4]. This model claims for the g-shift to show a similar frequency variation to that of the ESR linewidth. An existence of the g-shift change in the same frequency region as for the ESR linewidth has been confirmed in PANI-CSA film, but 30 MHz is too low to measure g-shift in TTF-TCNQ. The quantitative reproduction of the data by this model is not successful, but largely underestimate for TTF-TCNQ. Therefore, in the present status, there is no definite model to explain these data. It still remains as an open question.

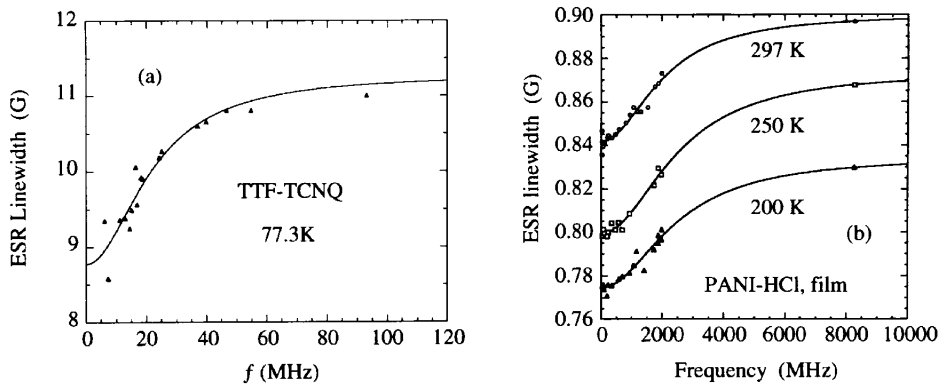

Fig. 12: (a) The frequency dependence of the ESR linewidth in TTF-TCNQ powder. (b) The frequency dependence of the ESR linewidth in PANI-HCl film cast from MNP solution.

7 Conclusion

With the several examples of organic conductive materials it was evidenced that the spin dynamics study is useful and powerful to investigate the dynamics of not only the spin, but also the charge carrier with spin as in the case of conduction electrons and polarons, including its anisotropy even in the polycrystalline materials. Since this field of experiments along the frequency axis in ESR is not fully developed yet, further refinement of experimental technique, analysis and interpretation are required and at the same time it has a possibility to give important information on the dynamics and electronic states of low dimensional conductive systems.

Acknowledgment

The author would like to express his thanks to Profs. H. Shirakawa, K. Akagi and Mr. M. Suezaki (Tsukuba Univ.) for collaboration on polyacetylene, especially preparation of highly oriented polyacetylene, to Drs. M. Nechtschein and J.-P. Travers (CENG, Grenoble) for stimulating discussion and collaboration on polyaniline, to Prof. S. Kazama and Dr. S. Masubuchi (Chuo Univ.) for collaboration on several conducting polymers, to Prof. G. Saito and Mr. M. Kubota for collaboration on charge transfer organic compounds, and to Prof. K. Kume, and present and old members of Kume's laboratory for their kind collaborations. This work was supported in part by Grant-in-Aid for Scientific Research from the Ministry of Education, Science, Sports and Culture (No.03640321 and No.07640487).

References

[1] K. Mizoguchi, *Jpn. J. Appl. Phys.*, vol. **34**, 1995, pp. 1-19.
[2] D. Lubzens, M.R. Shanabarger, and S. Schultz, *Phys. Rev. Lett.*, vol. **29**, 1972, pp. 1387.
[3] D.R. Fredkin and R. Freedman, *Phys. Rev. Lett.*, vol. **29**, 1972, pp. 1390-3.
[4] R. Freedman and D.R. Fredkin, *Phys. Rev.*, vol. **B11**, 1975, pp. 4847-58.
[5] C.A. Sholl, *J. Phys. C*, vol. **14**, 1981, pp. 447.
[6] M.A. Butler, L.R. Walker, and Z.G. Soos, *J. Chem. Phys.*, vol. **64**, 1976, pp. 3592.
[7] K. Mizoguchi and S. Kuroda, Magnetic Properties of Conducting Polymers, in *Handbook of Organic Conductive Molecules and Polymers*, ed. by H.S. Nalwa, John Wiley & Sons, Sussex, 1996, in press.
[8] M. Nechtschein, Electron spin dynamics, in *Handbook of Conducting Polymers*, ed. by T. Skotheim, Marcel Dekker, New York, 1996, in press.

[9] A. Abragam, *The Principles of Nuclear Magnetism*, Oxford Univ. Press, Oxford, 1961.
[10] G. Soda, D. Jerome, M. Weger, J. Alizon, G. Gallice, H. Robert, J.M. Fabre, and L. Giral, *J. de Phys.*, vol. **38**, 1977, pp. 931-48.
[11] W.G. Clark, K. Glover, M.D. Lan, and L.J. Azevedo, *J. Phys. Colloq.*, vol. **44**, 1983, C3 pp. 1493-9.
[12] K. Mizoguchi, *Makromol. Chem., Macromol. Symp.*, vol. **37**, 1990, pp. 53-66.
[13] K. Mizoguchi, K. Kume, and H. Shirakawa, *Mol. Cryst. Liq. Cryst.*, vol. **118**, 1985, pp. 459-62.
[14] J.S. Hyde, W. Froncisz, and T. Oles, *J. Mag. Res.*, vol. **82**, 1989, pp. 223.
[15] K. Mizoguchi, K. Kume, and H. Shirakawa, *Solid St. Commun.*, vol. **50**, 1984, pp. 213-18.
[16] K. Mizoguchi, K. Kume, S. Masubuchi, and H. Shirakawa, *Solid St. Commun.*, vol. **59**, 1986, pp. 465-8.
[17] K. Mizoguchi, K. Kume, and H. Shirakawa, *Synth. Met.*, vol. **17**, 1987, pp. 439-45.
[18] K. Mizoguchi, S. Komukai, T. Tsukamoto, K. Kume, M. Suezaki, K. Akagi, and H. Shirakawa, *Synth. Met.*, vol. **28**, 1989, pp. D393-8.
[19] K. Mizoguchi, S. Masubuchi, K. Kume, K. Akagi, and H. Shirakawa, *Phys. Rev.*, vol. **B51**, 1995, pp. 8864-73.
[20] B.R. Weinberger, E. Ehrenfreund, A. Pron, A.J. Heeger, and A.G. MacDiarmid, *J. Chem. Phys.*, vol. **72**, 1980, pp. 4749-55.
[21] M. Nechtschein, F. Devreux, R.L. Greene, T.C. Clarke, and G.B. Street, *Phys. Rev. Lett.*, vol. **44**, 1980, pp. 356-9.
[22] K. Holczer, J.P. Boucher, F. Devreux, and M. Nechtschein, *Phys. Rev.*, vol. **B23**, 1981, pp. 1051-63.
[23] M. Nechtschein, F. Devreux, F. Genoud, M. Guglielmi, and K. Holczer, *Phys. Rev.*, vol. **B27**, 1983, pp. 61-78.
[24] W.G. Clark, K. Glover, G. Mozurkewich, S. Etemad, and M. Maxfield, *Mol. Cryst. Liq. Cryst.*, vol. **117**, 1985, pp. 447.
[25] C.P. Slichter, *Principles of Magnetic Resonance*, vol. **1**, 3rd ed. Springer, Berlin, Heidelberg, 1989.
[26] K. Mizoguchi, H. Sakurai, F. Shimizu, S. Masubuchi, and K. Kume, *Synth. Met.*, vol. **68**, 1995, pp. 239-42.
[27] K. Mizoguchi, K. Kume, S. Masubuchi, and H. Shirakawa, *Synth. Met.*, vol. **17**, 1987, pp. 405-11.
[28] S. Kuroda, M. Tokumoto, N. Kinoshita, and H. Shirakawa, *J. Phys. Soc. Jpn.*, vol. **51**, 1982, pp. 693-4.
[29] S. Kuroda and H. Shirakawa, *Phys. Rev.*, vol. **B35**, 1987, pp. 9380-2.
[30] S. Kuroda, *Int. J. Mod. Phys. B*, vol. **9**, 1995, pp. 221-60.
[31] Y. Wada and J.R. Schrieffer, *Phys. Rev.*, vol. **B18**, 1978, pp. 3897-912.
[32] M. Ogata and Y. Wada, *Prog. Theor. Phys. Suppl.*, 1988, pp. 115-27.
[33] K. Maki, *Phys. Rev.*, vol. **B26**, 1982, pp. 4539-42.
[34] K. Maki, *Phys. Rev.*, vol. **B26**, 1982, pp. 2187-91.
[35] K. Maki, *Phys. Rev.*, vol. **B26**, 1982, pp. 2181-6.
[36] S. Jeyadev and E.M. Conwell, *Phys. Rev.*, vol. **B36**, 1987, pp. 3284-93.
[37] Y. Wada, *Progr. Theor. Phys. Suppl.*, vol. **113**, 1993, pp. 1-23.
[38] F. Devreux, *Phys. Rev.*, vol. **B25**, 1982, pp. 6609.
[39] S. Kivelson, *Phys. Rev.*, vol. **B25**, 1982, pp. 3798-21.
[40] D. Baeriswyl, D.K. Campbell, and S. Mazumdar, An overview of the theory of π-conjugated polymers, in *Conjugated Conducting Polymers*, vol. **102**, ed. by H.G. Kiess, Springer-Verlag, Berlin, Heidelberg, 1992, pp. 107.
[41] K. Mizoguchi, M. Nechtschein, J.-P. Travers, and C. Menardo, *Phys. Rev. Lett.*, vol. **63**, 1989, pp. 66-9.

[42] K. Mizoguchi, M. Nechtschein, J.P. Travers, and C. Menardo, *Synth. Met.*, vol. **29**, 1989, pp. E417-24.
[43] K. Mizoguchi, M. Nechtschein, and J.-P. Travers, *Synth. Met.*, vol. **41**, 1991, pp. 113-16.
[44] K. Mizoguchi and K. Kume, *Solid St. Commun.*, vol. **89**, 1994, pp. 971-5.
[45] A.G. MacDiarmid, J.C. Chiang, M. Halpern, W.S. Huang, S.L. Mu, N.L.D. Somasiri, W.Q. Wu, and S.I. Yaniger, *Mol. Cryst. Liq. Cryst.*, vol. **121**, 1985, pp. 173.
[46] M. Reghu, Y. Cao, D. Moses, and A.J. Heeger, *Synth. Met.*, vol. **57**, 1993, pp. 5020-5.
[47] A.P. Monkman and P.N. Adams, *Synth. Met.*, vol. **41-43**, 1991, pp. 627.
[48] J.P. Pouget, M. Laridjani, M.E. Jozefowicz, A.J. Epstein, E.M. Scherr, and A.G. MacDiarmid, *Synth. Met.*, vol. **51**, 1992, pp. 95-101.
[49] J.P. Pouget, Z. Oblakowski, Y. Nogami, P.A. Albouy, M. Laridjani, O. E.J., Y. Min, A.G. MacDiarmid, J. Tsukamoto, T. Ishiguro, and A.J. Epstein, *Synth. Met.*, vol. **65**, 1994, pp. 131-40.
[50] J.P. Pouget, C.-H. Hsu, A.G. MacDiarmid, and A.J. Epstein, *Synth. Met.*, vol. **69**, 1995, pp. 119-20.
[51] C. Jeandey, J.P. Boucher, F. Ferrieu, and M. Nechtschein, *Solid St. Commun.*, vol. **23**, 1977, pp. 673.
[52] A.J. Epstein, J.M. Ginder, F. Zuo, R.W. Bigelow, H.-S. Woo, D.B. Tanner, A.F. Richter, W.-S. Huang, and A.G. MacDiarmid, *Synth. Met.*, vol. **18**, 1987, pp. 303-9.
[53] K. Mizoguchi and K. Kume, *Synth. Met.*, vol. **69**, 1995, pp. 241-2.
[54] E. Houzé and M. Nechtschein, submitted to Phys. Rev. **B**.
[55] E.J. Oh, Y. Min, J.M. Wiesinger, S.K. Manohar, E.M. Scherr, P.J. Prest, A.J. MacDiarmid, and A.J. Epstein, *Synth. Met.*, vol. **55-57**, 1993, pp. 977.
[56] K. Mizoguchi, M. Honda, N. Kachi, F. Shimizu, H. Sakamoto, K. Kume, S. Masubuchi, and S. Kazama, *Solid St. Commun.*, vol. **96**, 1995, pp. 333-7.
[57] K. Mizoguchi, M. Honda, S. Masubuchi, S. Kazama, and K. Kume, *Jpn. J. Appl. Phys.*, vol. **33**, 1994, pp. 971-5.
[58] S. Masubuchi, S. Kazama, K. Mizoguchi, H. Honda, K. Kume, R. Matsushita, and T. Matsuyama, *Synth. Met.*, vol. **57**, 1993, pp. 4962-7.
[59] R.J. Elliott, *Phys. Rev.*, vol. **96**, 1954, pp. 266-79.
[60] S. Masubuchi and S. Kazama, *Synth. Met.*, vol. **74**, 1995, pp. 151-8.
[61] K. Mizoguchi, K. Misoo, K. Kume, K. Kaneto, T. Shiraishi, and K. Yoshino, *Synth. Met.*, vol. **18**, 1987, pp. 195-8.
[62] F. Moraes, D. Davidov, M. Kobayashi, T.C. Chung, J. Chen, A.J. Heeger, and F. Wudl, *Synth. Met.*, vol. **10**, 1985, pp. 169-79.
[63] S. Masubuchi and S. Kazama, *Synth. Met.*, vol. **69**, 1995, pp. 315-16.
[64] S. Kivelson and A.J. Heeger, *Synth. Met.*, vol. **22**, 1988, pp. 371-84.
[65] F. Shimizu, K. Mizoguchi, S. Masubuchi, and K. Kume, *Synth. Met.*, vol. **69**, 1995, pp. 43-4.
[66] F. Shimizu, Thesis: Tokyo Metropolitan Univ., 1994.
[67] D. Billaud, J. Ghanbaja, J.F. Marêché, E. McRae, and C. Goulon, *Synth. Met.*, vol. **28**, 1989, pp. D147-54.
[68] P. Bernier, C. Fite, A. El-Khodary, F. Rachdi, K. Zniber, H. Bleier, and N. Coustel, *Synth. Met.*, vol. **37**, 1990, pp. 41.
[69] F. Rachdi and P. Bernier, *Phys. Rev.*, vol. **B33**, 1986, pp. 7817-19.
[70] L. Kispert, J. Joseph, G.G. Miller, and R.H. Baughman, *Mol. Cryst. Liq. Cryst.*, vol. **106**, 1984, pp. 418.
[71] P. Lauginie, H. Estrade, J. Conard, D. Guerard, P. Lagrange, and M. El Makrini, *Physica B & C*, vol. **99**, 1980, pp. 514-20.
[72] K. Tanigaki, M. Kosaka, T. Manako, Y. Kubo, I. Hirosawa, K. Uchida, and K. Prassides, *Chem. Phys. Lett.*, vol. **240**, 1995, pp. 627.